Mass and heat balance of snowpatches in Basen nunatak, Dronning Maud Land, Antarctica, in summer

Matti LEPPÄRANTA, Onni JÄRVINEN, Elisa LINDGREN

Department of Physics, University of Helsinki, Helsinki, Finland
E-mail matti.lepparanta@helsinki.fi

ABSTRACT. An experimental study concerning the mass and heat balance of snowpatches was performed during the Finnish Antarctic Research Programme (FINNARP) 2004 and 2010 summer expeditions to Basen nunatak (73°03′ S, 13°25′ W). Data were collected from a snow stake line, snow pits and automated weather and snow recording systems. One 100 m perennial snowpatch and several smaller seasonal patches (<10 m) were monitored. Snow thickness decreased by 4.0–6.3 mm d^{-1} due to sublimation, compression and, close to lateral boundaries, meltwater runoff. The vertical mass loss was 1–2 mm snow water equivalent (SWE) d^{-1} and the lateral decay was ~10 cm d^{-1}. The net radiation was 20.2 W m^{-2} and the mean latent heat flux was –15.5 W m^{-2}. The mean surface energy flux was 4.9 W m^{-2} and the heat loss to the ground was 1.5 W m^{-2}. Thin snow decayed faster due to surface thermomechanical erosion and melt from the bottom where the soil was heated by the solar radiation. Between the summers of 2004 and 2010, the thickness of the perennial snowpatch decreased by 230 mm.

1. INTRODUCTION

Snow covers nearly all surfaces in Antarctica, including the ice cover of the surrounding seas, and is the principal modulator of the surface energy budget. Snowfall represents the inflow of mass into the snow and ice storage of the continent, which acts as one controller of the global sea-level elevation. Nunataks are striking features in the Antarctic landscape. They puncture the ice sheet and rise high above it, up to several hundred metres in western Dronning Maud Land. Nunatak surfaces contain bare areas, short-term transient snow spots, seasonal and perennial snowpatches and small glaciers. The annual mass balance of the seasonal snowpatches is zero, by the definition of seasonality, determined by precipitation, sublimation, wind-driven transport of snow and summer runoff of meltwater. The annual mass balance of perennial patches follows the local climate evolution.

The mass and heat balance of nunatak snowpatches is of interest in the research of Antarctic snow and climate in general. Wind-driven transport of snow and the sublimation–deposition mechanisms influence the redistribution of snow mass over larger regions. Snowpatches may decay by melting and produce runoff, which acts as a source of moisture for the soil. The runoff may form drainage systems, which contain liquid water ponds with specific ecosystems (Keskitalo and others, 2013). Small nunatak glaciers may contain very old ice since net accumulation of snow may be very slow. The influence of climate variations should show up clearly in the snow mass balance of nunataks. However, very little research has been undertaken on the snow on nunataks.

To date, there have only been a few studies concerning seasonal snowpatches on land. In addition to nunataks, snowpatches are a common characteristic in high mountains and tundra. Watson and others (1994) studied the evolution of summer snowpatches in Scotland, and Mott and others (2013) investigated this topic in the Swiss Alps. Berrisford (1991) showed that mechanical weathering is enhanced under seasonally late-lying and perennial snowpatches. Gooseff and others (2003) studied the influence of snowpatches on biochemical processes in the soil in the McMurdo Dry Valleys, Antarctica. Their results showed that seasonal snowpatches may be an important source of moisture and may control habitats of soil biota in extreme conditions. The connections between summer snowpatches and vegetation have been examined in the tundra in Finnish Lapland (Eurola and others, 2004).

To obtain an understanding of the dynamics of nunatak snowpatches, field investigations were performed by the Finnish Antarctic Research Programme (FINNARP) during the 2004 and 2010 austral summer expeditions to Basen nunatak, western Dronning Maud Land. Basen nunatak is located at 73°03′ S, 13°25′ W, 125 km south of the shelf edge in the Weddell Sea. It is the most northern nunatak of the Vestfjella mountain range, which is situated near the grounding line and aligned approximately parallel to the coast. The research work was conducted from Aboa research station, which is located on Basen close to the field sites. Several investigations of snow accumulation and stratigraphy have been made on the ice sheet in western Dronning Maud Land from the shelf edge up to the polar plateau (e.g. Isaksson and Karlén, 1994; Kärkäs and others, 2002; Reijmer and Van den Broeke, 2003; Richardson-Näslund, 2004; Granberg and others, 2009; Ingvander and others, 2011); however, the snow on nunataks was not included in those investigations.

Our work is based on an experimental study of nunatak snowpatches. The data have been analysed focusing on the mass and heat balance and decay rates of the snowpatches in summer. The mass and heat balances were determined independently from a snow stake line and weather data, resulting in good agreement. In addition, the individual components of the mass and heat balances were evaluated. The loss of snow was due to sublimation and meltwater runoff. Here we present the final results.

2. MATERIALS AND METHODS

2.1. Site

The research base was Aboa station on Basen nunatak. The horizontal cross section of Basen is ~4 km × 2 km, with the

https://doi.org/10.3189/2013JoG12J236 Published online by Cambridge University Press

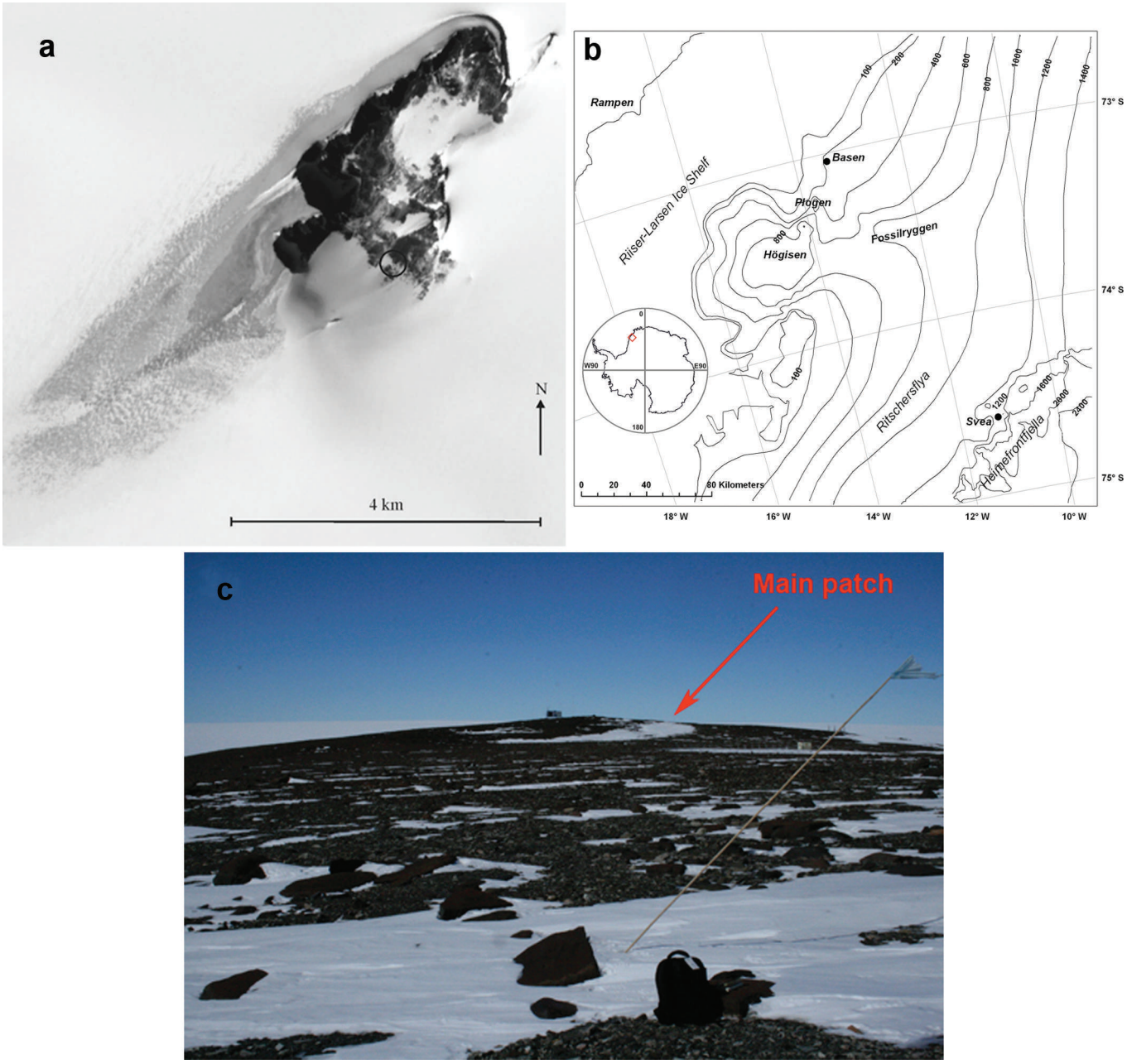

Fig. 1. (a) Terra/ASTER (Advanced Spaceborne Thermal Emission and Reflection Radiometer) image from 8 November 2001 showing Basen nunatak (©NASA). (b) A map of western Dronning Maud Land showing the location of Basen nunatak. (c) A photograph of the snowpatch study area on 10 December 2010. The main patch is located on the slope as shown and the small patches are between the main patch and the flagpole in front. The distance from the flagpole to the main patch is ~400 m. The hut on the distant top is the Aboa AWS.

long axis oriented in the northeast–southwest direction (Fig. 1a and b). The field experiments were carried out during the 2004/05 and 2010/11 austral summers (December–January). The main snowpatch of the field study was located at 73°02.5′ S, 13°24.2′ W, 480–490 m a.s.l. (Kanto and others, 2007). This snowpatch was perennial and medium-sized: its horizontal extent was 100 m and its thickness was ~1 m at maximum. Its age is unknown but it has existed at least since the 1990s. In the neighbourhood, at distances up to 300 m from the main site, the decay of small seasonal snowpatches (horizontal extent <10 m) was monitored. Figure 1c shows the study area with the main snowpatch on the facing slope and small snowpatches between. The automatic weather station (AWS) of Aboa is located 100 m from the main site at 73°02.481′ S, 13°24.075′ W, 498 m a.s.l.

The annual net accumulation of snow is 150–250 mm snow water equivalent (SWE), or 150–250 kg m^{-2} in terms of the annual mass accumulation, over the nearby ice sheet (Isaksson and Karlén, 1994; Kärkäs and others, 2002; Granberg and others, 2009). With the average surface layer density of 400 kg m^{-3} this corresponds to a snow layer ~500 mm thick. Net snow accumulation on Basen is driven by precipitation, snowdrift, sublimation and meltwater runoff. In 1989–2001 the mean annual air temperature was –15°C at Aboa AWS, and the monthly means ranged between –21.9°C in August and –5.2°C in January (Kärkäs, 2004). Wind climatology showed an annual cycle where the annual mean wind speed was 7.7 m s^{-1} and the minimum and maximum monthly mean winds were 5.4 m s^{-1} in January and 9.0 m s^{-1} in August, respectively. The ratio of gust speed to mean wind speed was 1.5–1.6 : 1. The

https://doi.org/10.3189/2013JoG12J236 Published online by Cambridge University Press

predominant wind direction was 30° (northeast), with 76% of all winds from the sector 20–40°. This sector included the strongest wind speeds, at strongest from 20°. A secondary peak showed up in the sector 190–210° (south-southwest) due to katabatic winds from the central continent. Thus the distribution of wind direction was largely due to the local topography (nunatak), which is the single most important factor in shaping the Antarctic surface wind regime (Parish, 1988).

2.2. Methods

At the main site, a snow stake line was monitored, snow pits were excavated at regular intervals, and automated recording systems were deployed for the radiation balance and snow temperature. The stake line was established at the beginning of the first field season (Fig. 2), containing 16 snow stakes at 5 m spacing. The direction of the line was 333° (northwest–southeast) located on a slope with tilt of 0.085 ± 0.040 ($4.8° \pm 2.3°$) along the line and 0.137 ± 0.032 ($7.8° \pm 1.8°$) across the line; stake 1 was at the highest altitude. Most stakes were still standing straight at the beginning of December 2010. The initial thickness at the stakes was in the range 200–800 mm. Snow thickness was monitored at 1–2 day intervals at the snow stakes, and at 3–7 day intervals a snow pit was excavated. The accuracy of the snow surface level read from the stakes is 5 mm. Thermal expansion due to temperature variations within 10°C influences the snow surface level here at most by 1 mm.

Basic physical properties of snow were measured from the snow pits. One vertical wall was left clean and the top of it untouched. The visible stratigraphy was recorded. Profiles were then determined at 20–100 mm intervals for temperature, density, size and shape of snow grains, and volume fraction of liquid water. The temperature profiles were measured using a Pt1000 temperature sensor with an accuracy of 0.2°C. Snow density was measured directly using a cylinder sampling kit with a volume of 0.25 dm^3 (diameter 50 mm) and a spring balance giving an estimated accuracy of 10 g dm^{-3}. Snow grains were photographed in the field using a special camera stand (Pihkala and Spring, 1985) and classified using the photographs according to the system of Fierz and others (2009). The reported snow grain size is the greatest extension of a grain. Liquid water content was estimated from the complex electric permittivity, which was measured with a snow fork manufactured by Toikka Ltd, Finland (Sihvola and Tiuri, 1986).

Automated recording systems were deployed at the snow site. In FINNARP-2004, a Kipp & Zonen NR Lite (spectral range 0.2–100.0 μm) was used for net radiation and a Middleton EP-16 pyrano-albedometer system (spectral range 0.30–3.0 μm) was used for incoming and outgoing solar radiation. The sensitivity of the NR Lite is 0.65 W m^{-2}, directional error is <3% and at high wind speed a correction of 5–10% is applied in the recordings. The Middleton system has a nonlinearity of ±0.5%, directional response of ±1.5% and tilt response of ±0.25%. The main question with regard to accuracy is in the sensor orientation, which needs to be horizontal. The sensor tripods were placed on snow and to protect them from sinking and tilting they were attached to white plywood plates, which were covered with snow. The orientation was controlled daily. Estimating the orientation to be horizontal within 3° (corresponding to a sensor tilt <1 : 20), the accuracy of the radiation recordings can be taken as 5 W m^{-2}. The tripods were deployed between snow stakes 2 and 3. They stored data at 1 min intervals, and 1 hour averages were calculated from the measurements to evaluate the heat balance.

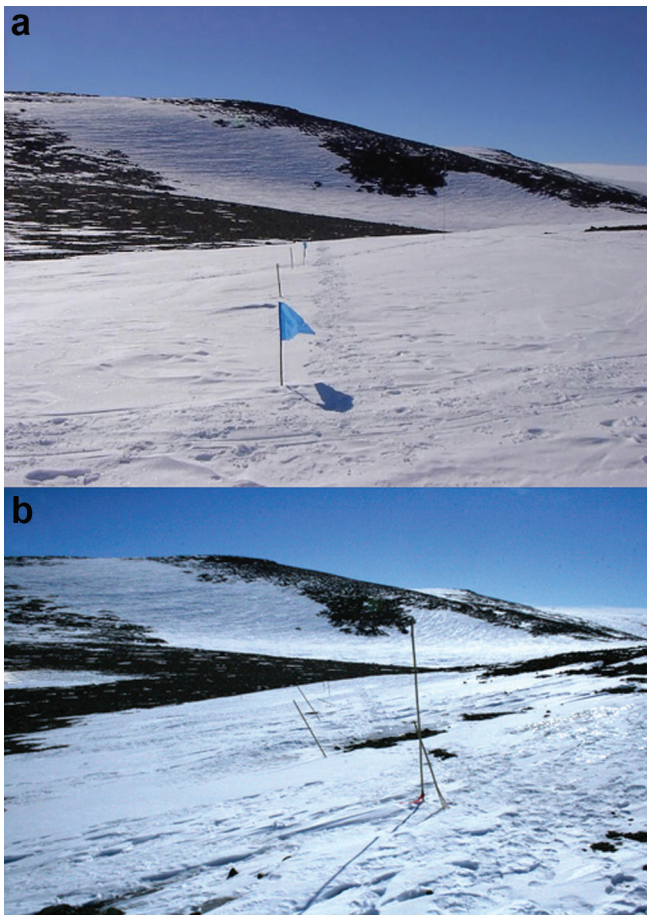

Fig. 2. Aboa snow stake line on (a) 14 December 2004 and (b) 10 December 2010.

Cylinder-shaped MDS-L photosynthetically active radiation (PAR) sensors (Alec Electronics Co. Ltd, Tokyo, Japan) 115 mm in length and 18 mm in diameter were deployed inside the snowpack to record the penetration of sunlight. These sensors had been calibrated by the manufacturer for hemispheric scalar quantum PAR irradiance, with a claimed accuracy of 2 W m^{-2}. Since radiation inside the snowpack is diffuse, the orientation of the sensors is not a very critical factor. In addition, in 2004 a thermistor pipe was deployed between snow stakes 7 and 8 to record the temperature profile of the snowpack. The accuracy was 0.2°C. The temperatures were recorded at 10 min intervals, and 1 hour averages were calculated for the data analyses.

The Aboa AWS (model: Vaisala MILOS 500) provided air pressure, air temperature and humidity, wind speed and direction, and incoming solar radiation at 1 hour intervals. The station belongs to the Finnish Meteorological Institute, which controls the data quality. The instrumental levels are 2 m for the temperature and humidity and 5 m for the wind. The instruments were in a mast on the side of a small hut (see Fig. 1c), with the wind sensor well above the roof so as not to be disturbed by the body of the hut. The immediate surroundings of the hut were bare rock, located on a local elevation maximum at ~100 m from the main snowpatch. According to the manufacturer, the accuracies are 0.2°C for the air temperature, 3% units for the relative humidity and

https://doi.org/10.3189/2013JoG12J236 Published online by Cambridge University Press

0.5 m s^{-1} for the wind speed. Short gaps ($\leq$3 hours) in the data were filled by spline interpolation. There were a few gaps of 1–2 days, which were left untouched and appear as cuts in the data plots.

The surface temperature was estimated from the thermistor pipe and the AWS data, requiring continuity of the heat flow across the snow surface. This is the weakest item in the data, with an estimated accuracy of 1°C. The sublimation and the turbulent heat fluxes could then be estimated from the bulk turbulent transfer formula.

In addition to the main snow site, the dynamics of minor snowpatches was monitored for their thickness and area. In summer 2010/11 several small seasonal patches were chosen from the valley down from the main site (Fig. 1c). Their size ranged from 1 to 10 m across and the snow thickness was a maximum of ~250 mm at the beginning of December. The patches were equipped with a stake in the centre for the vertical decay, and their lateral decay was monitored by surface photography. The estimated accuracies of their thickness and lateral extent are 5 mm and 1 cm, respectively. All the small patches decayed during the summer.

3. MASS BALANCE OF SNOW

3.1. Main patch

The mass balance of a snow cover can be written as (e.g. Paterson, 1994)

$$\frac{\mathrm{d}M}{\mathrm{d}t} = P - E - R + Y \tag{1}$$

where M is snow mass per unit area, t is time, P is precipitation, E is sublimation, R is runoff and Y is transport due to wind-driven snowdrift. Precipitation and snowdrift are shown as separate quantities for clarity as they represent different physics. These terms are expressed in SWE per time. The same snowline was used in both field seasons (Fig. 2), and in the 6 years between expeditions there had been a net loss of snow. The average snow thickness on 11 December was 230 mm less in 2010 than in 2004 (or 90 mm less in terms of SWE). Comparing the snow stake line between the end of January 2005 and the end of January 2011, snow thickness was 284 mm less. At the start of the line (stakes 1–5) in 2010 the snow was thin and the old stakes were tilting and in the course of the summer the snow was lost from these stakes.

Precipitation is almost always solid over Basen. Since the mid-1990s, the only known major liquid precipitation events have occurred in January 2003 and 2010. These seasons are not included here, but the implications of the later event were seen in the main snowpatch in the following summer, i.e. in our second field season. In both summers studied, snowfalls were rare and new snow was soon blown away by wind so that accumulation of new snow was marginal except at the end of January 2005. Drifting of older snow was not observed in the first study season, but in the second season a small amount was noted at the beginning of the study period. Thus precipitation and snowdrift made minor contributions to the summer mass balance and Eqn (1) indicates that snow was then lost due to sublimation and runoff. At the end of January 2011 there was an indication of minor snow accumulation due to deposition of atmospheric moisture.

Close to the lateral boundaries of the snowpatches where the snow cover was thin the presence of meltwater runoff was noted. This was largely produced by melting at the snow–soil interface, to where heat was transferred due to penetration of sunlight through the thin snow and advection from the nearby bare soil. It was estimated from the data that the former mechanism is dominant (see Section 4.3). The snow-pit profiles were dug into snow that was ~0.5 m thick where snowmelting did not become strong enough to initiate runoff, rather a small amount of moist snow was observed just beneath the surface. At the warmest summer peak the volume fraction of liquid water was <1%. Later, this meltwater refroze, resulting in melt–freeze metamorphosis within the snowpack. It is apparent that runoff, if any, was very small in the thick snow area and it was evident that sublimation caused most of the loss of snow in this area.

The frozen ground in snow-free areas melted down to 0.5 m depth in summer and was moist. The water source was the ice in the frozen ground at site and meltwater runoff from snowpatches. In the study area no liquid water ponds or pools were seen, but higher up on Basen several were present (Keskitalo and others, 2013).

Snow mass can be expressed as $M = (\widetilde{\rho}_s/\rho_w)h$ SWE, where $\widetilde{\rho}_s$ is the vertical mean density of snow, ρ_w = 1000 kg m^{-3} is the water density and h is the snow thickness. Equation (1) can then be transformed to

$$\frac{\mathrm{d}h}{\mathrm{d}t} = -\frac{h}{\widetilde{\rho}_s}\cdot\frac{\mathrm{d}\widetilde{\rho}_s}{\mathrm{d}t} + \frac{\rho_w}{\widetilde{\rho}_s}(P - E - R + Y) \tag{2}$$

Thus snow thickness changes due to packing and net mass change are given by the first and second terms, respectively, on the right-hand side of Eqn (2). Our observations provide the thickness change and packing and the mass balance then comes as the residual.

The decrease in snow thickness at the snow stakes is shown in Figure 3a for both summers. In 2004/05 the total decrease in snow thickness was 120–300 mm; snow thickness at stake 16 was initially 75 mm and the snow was gone on 19 January 2005. In December 2004 the rate of decrease in snow thickness averaged 4 mm d^{-1} (Fig. 3b). The summer was warmest during 1–20 January 2005 and the rate peaked at 15 mm d^{-1}. Thereafter the thickness decreased at a slower rate (1–2 mm d^{-1}) and also accumulation of new snow occurred on 2 days. The time series of the snow thickness showed good correlation between the different stakes.

In summer 2010/11, the decrease in snow thickness was 250–500 mm throughout the whole season (3 December–29 January); stakes 1–5, 10 and 13–16 lost their snow before the end of the experiment (Fig. 3a). The rate of decrease in snow thickness averaged 6.3 mm d^{-1} (Fig. 3b). The highest values were recorded at stakes 12 and 13 and the summer was again warmest during 1–20 January. The peak rate was 20 mm d^{-1}. The daily changes in snow thickness showed a systematically stronger decrease in 2010/11 than in 2004/05. There was one major snow accumulation event in 2010/11 followed by a rapid loss of new snow, which was blown away by wind.

Compression of the snow layer due to mechanical forcing or densification in melt–freeze metamorphosis must be eliminated to obtain the mass balance from the snow thickness data. The first term on the right-hand side of Eqn (2) represents the influence of compression. In the summer the evolution of snow density was near-linear (Table 1). Hence, the solution of Eqn (2) is

$$h = \frac{\rho_{s0}}{\rho_{s0} + \gamma t}h_0 + \frac{\rho_w}{\rho_{s0} + \gamma t}(M - M_0) \tag{3}$$

where h_0, ρ_{s0} and M_0 are the initial thickness, density and

https://doi.org/10.3189/2013JoG12J236 Published online by Cambridge University Press

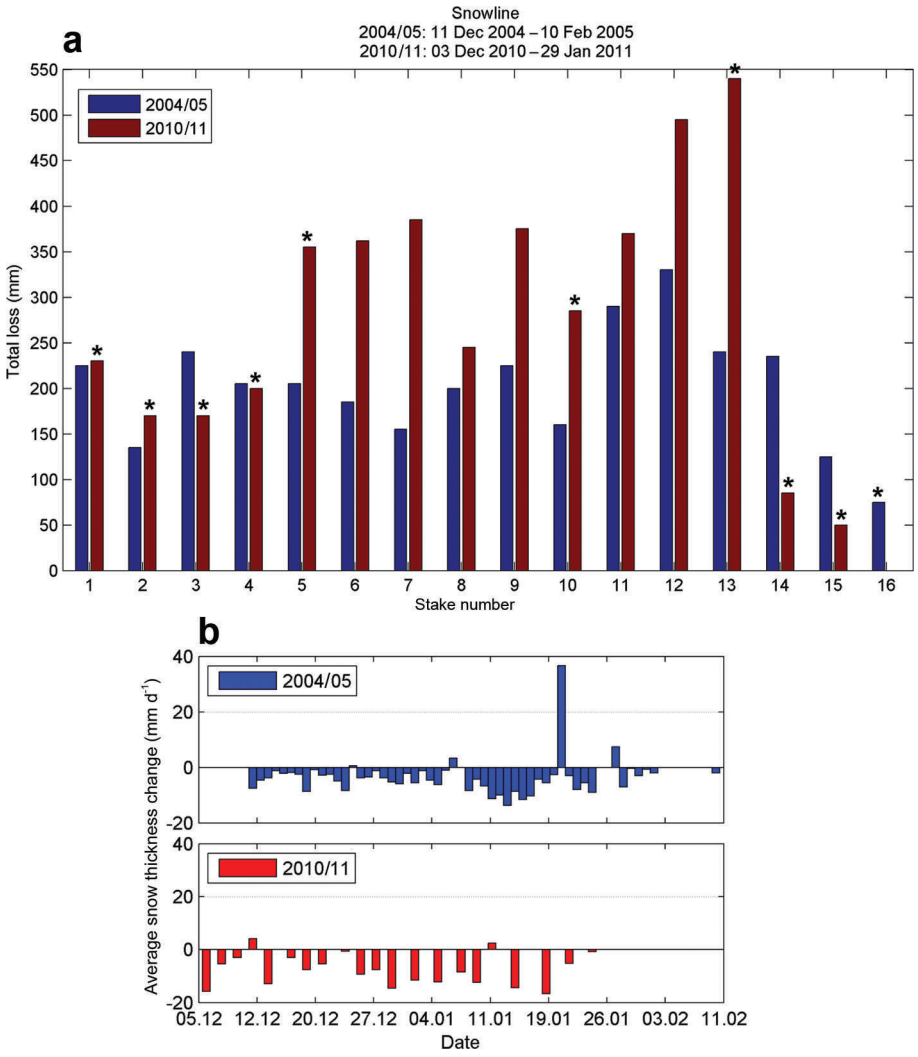

Fig. 3. Snow thickness change in austral summers 2004/05 and 2010/11 in the snow stake line. (a) December–January at each snow stake 1–16; asterisks indicate that the snow had all gone before the end of the experiment. (b) Time series of daily average changes across the whole snowline. Date format is day.month.

mass (SWE) of snow at time $t=0$ and $\gamma = \mathrm{d}\tilde{\rho}_s/\mathrm{d}t = \text{constant}$ is the packing rate of snow.

In 2004/05 the vertically averaged density of snow ranged from 320 to 470 kg m^{-3} (Table 1). A trend line was fitted to the densities resulting in $\rho_{s0} = 335$ kg m^{-3} and $\gamma = 2.65$ kg m^{-3} d^{-1}, where the initial time $t=0$ is 14 December 2004. The last measurement was based on the snow fork data and was excluded from the fitting; for that day the trend predicts 460 kg m^{-3}, which is 10 kg m^{-3} less than the value given in Table 1. Equation (3) was then used to extract the compression effect from the observed decrease in snow thickness, resulting in 50–200 mm (Fig. 4), which accounted for a little more than half of the change in the snow thickness.

The structure of the snow cover was somewhat different in 2010/11. Four snow pits were dug in the main snowpatch. They revealed a thick, hard, refrozen layer under the surface layer (0–15 mm); snow density samples were taken of the surface layer. The refrozen layer that was already observed in the early season was possibly caused by the major liquid precipitation event in January 2010. On 3 December, the density of the surface snow layer was 245 kg m^{-3} and on 14 December it was 385 kg m^{-3}. The low density on 3 December was due to a 3 mm thick surface hoar layer. Later, the whole snowpack transformed into a hard crust and density measurements were no longer conducted.

We can examine the influence of snow compression in summer 2010/11 indirectly, since several stakes lost all their snow. This is, however, a rough approximation, since snow

Table 1. Thickness and mean density of snow at the snowline in the snow pits. Density has been determined directly from the mass of sample volume (except in one case)

Date	Summer 2004/05 total		Summer 2010/11 top layer	
	Thickness	Density	Thickness	Density*
	mm	kg m^{-3}	mm	kg m^{-3}
3 Dec	–	–	320	245
14 Dec	500	320	240	385
24 Dec	600	364	220	–
28 Dec	500	384	–	–
1 Jan	700	409	160	–
10 Jan	550	383	120	–
30 Jan	400	470†	50	–

*15 cm thick surface layer. †From relative permittivity.

https://doi.org/10.3189/2013JoG12J236 Published online by Cambridge University Press

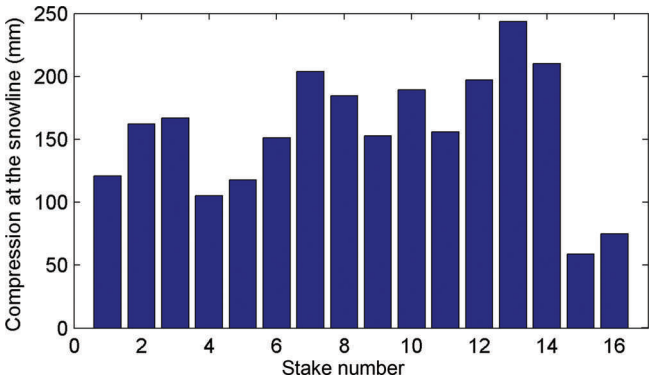

Fig. 4. The influence of compression on the decrease in snow thickness at the snow stakes from 14 December 2004 to 30 January 2005.

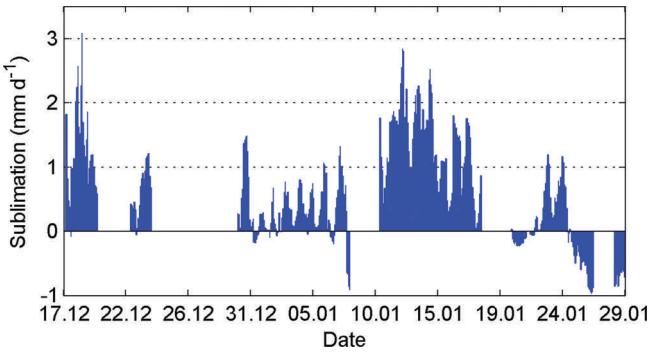

Fig. 5. Sublimation in December 2004–January 2005 based on the atmospheric surface layer data and the estimated surface temperature. A full turbulence model was used, accounting for the stability of the stratification. Date format is day.month.

decay speeds up when the snow cover has become thin enough for sunlight to penetrate through it and start to warm the ground. Of the 16 stakes, 10 lost all snow, the first on 14 December and the last on 10 January. The rate of decrease in snow thickness at these stakes was 4–8 mm d^{-1}, the average was 6.3 mm d^{-1} and the standard deviation was 1.8 mm d^{-1}. This was about the same as the decrease in snow thickness at the stakes where not all snow was lost. Consequently, snowpacking was a minor factor in summer 2010/11. This is likely because in the beginning the snow cover was already mostly hard crust, with higher compressive strength than in 2004/05.

Sublimation of snow can be estimated independently from the atmospheric surface layer data using turbulent transfer models. Here the bulk formula for the transfer of water vapour is employed (e.g. DeWalle and Rango, 2008):

$$\rho_w E = \rho_a C_E (q_0 - q_a) U_a \quad (4)$$

where $\rho_a = 1.3\ \mathrm{kg\ m^{-3}}$ is the density of air (0°C), C_E is the turbulent transfer coefficient of water vapour, q_0 and q_a are the specific humidities at the surface and air, respectively, and U_a is the wind speed. The specific humidity at the surface can be taken as the saturation level corresponding to the surface temperature. The transfer coefficient depends on the surface roughness and the stability of atmospheric surface layer stratification. In neutral stratification, the coefficient can be taken as a constant, $C_E = 1.3 \times 10^{-3}$. Then, if the humidity is 75%, the air and surface temperature are both equal to 0°C and the wind speed is 10 m s^{-1}, the resulting sublimation will be 1.4 mm SWE d^{-1}, implying a 3–4 mm decrease in the thickness of snow per day.

Sublimation was estimated for the 2004/05 summer using the snow stake line and Aboa AWS data. Surface temperature was estimated by assuming continuity of the heat flux through the air–snow interface. A linearized surface heat flux formulation was employed (Leppäranta and Myrberg, 2009). To obtain the sublimation, the flux-profile method of Launiainen and Vihma (1990) was used. The input data to this algorithm are the geometric roughness of the surface, and air temperature, humidity and wind speed at two or more heights, and the algorithm accounts for the influence of the stability of the stratification of the atmospheric surface layer. The result is shown in Figure 5. The average level of sublimation was ~1 mm SWE d^{-1} and the peaks reached up to 3 mm SWE d^{-1}, which correspond to a decrease in snow thickness of 2.5 and 7.5 mm d^{-1}, respectively. There was a strong daily cycle, with the nighttime level ~0.03 mm h^{-1}, 50% lower than the daytime level. The total sublimation during the summer was 50 mm SWE, which is close to the estimated average compression effect.

Assuming neutral stratification with the constant exchange coefficient would introduce small errors in the summertime compared with the stability correction. It is clear that, in winter, when the stratification is dominantly stable, the neutral stratification approach will lead to much more biased results. The algorithm of Launiainen and Vihma (1990) evaluates the hydrodynamic surface roughnesses of momentum, temperature and humidity based on the given geometric surface roughness, which was estimated as 15 cm for the site region covering the snowpatch and a bare rock field. A sensitivity analysis by changing the geometric surface roughness to 1 cm resulted in <10% change to the turbulent fluxes, considered here as a small factor. The 1 cm level corresponds to the conditions at the beginning of summer, and during summer deterioration of the snowpack the geometric surface roughness develops into a more rough and anisotropic state with penitents inclined toward the solar noon direction (Fig. 6).

The obtained sublimation was consistent with the result for the change in snow thickness and compression of the snowpack. On average, sublimation accounted for almost half of the change in snow thickness and it was at its largest at the peak of the summer. A few negative cases were obtained, mainly at the end of January, corresponding to deposition of atmospheric moisture (the occurrence of the deposition was confirmed by visual observations). The level of estimated sublimation is high, but in the Antarctic marginal regions such levels have previously been observed in summer (Van den Broeke and Bintanja, 1995).

Much more snow was lost in summer 2010/11 than in 2004/05. A possible reason for this is that the snow was thinner in the latter season, since there is a positive feedback to snow decay from the soil as soon as the solar radiation reaches the ground and starts warming and melting snow from the bottom. This feedback is strengthened by mechanical erosion at the surface due to formation of penitents (Fig. 6). The penitents were tilted and oriented toward the north-northeast sector, formed by the solar radiation (Lliboutry, 1954). The hollows became deeper in January and snow thickness at the stakes was no longer so well defined. Collapsing penitents cause sudden drops in

https://doi.org/10.3189/2013JoG12J236 Published online by Cambridge University Press

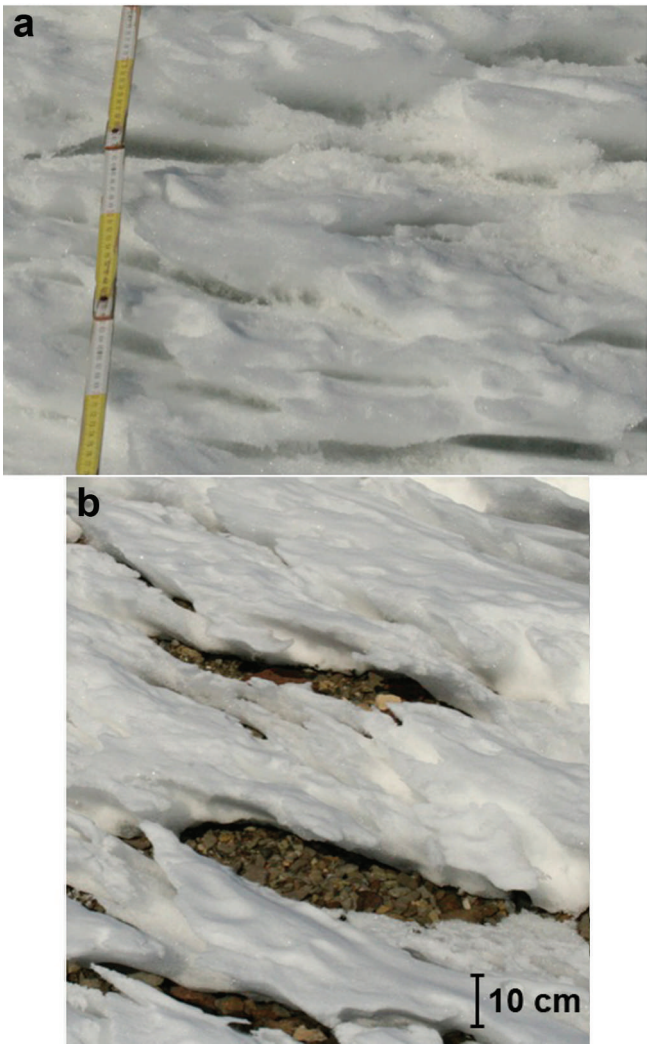

Fig. 6. Penitents on the snow surface in the main snowpatch. (a) Penitents start to form (white/yellow sections on the meter stick are each 10 cm). (b) In thin snow the hollows have reached the soil surface.

snow thickness. The hollows could reach bare ground even when the snow thickness was still 200–300 mm.

Figure 7 shows how the edge of the snowpatch near stake 3 was retarding during summer 2010/11. On 20 December one marker (stake 3a) was placed at the edge of the snowpatch and a stake was placed in the snow 2 m from the edge. The edge retarded steadily by 5–20 cm d^{-1} until 22 January 2011, reaching a total of 270 cm in 33 days. The depth of snow at stake 3a and the slope of the snow thickness were initially 180 mm and 1 : 10, respectively. Snow thickness at the edge stake had decreased to 150 mm by 30 December, 100 mm by 10 January and zero by 19 January. Thereafter the snowpatch retarded fast laterally. Over the summer, at the edge, the average decrease in snow thickness was 6 mm d^{-1} while at the snowline the average was 6.3 mm d^{-1}. When the snow thickness had decreased to ~100 mm, the decay became significantly faster.

3.2. Small patches

Systematic monitoring of small snowpatches was performed in summer 2010/11. The section across the patchy snowfield was a continuation of the snow stake line in the main snowpatch (Fig. 1c). The line crossed the valley northwest of Aboa from snowline stake 16 to 73°02.344′ S, 13°24.522′ W and its total length was 270 m. The thickness and area of 14 selected patches were monitored by photography and snow stakes at 2 day intervals (one stake in the centre of each small snowpatch). The observations were started on 4 December 2010. The size of the monitored patches was 1–10 m and the distance between them was 10–30 m. Initially the thickness of snow at the stakes ranged from 40 to 260 mm. Figure 8 shows an example of photographs from one patch during the course of the decay process.

During the first few days, some snow drifted away during stormy days (5 and 7 December). The snow had disappeared from all patches by the beginning of January (Fig. 9) and no further new snow accumulated. Winds blew predominantly from northerly directions, which was reflected in accumulation of snow on the lee side of topographical obstacles such as large stones. The rate of decay of the patches was 5–10 mm d^{-1} of snow thickness, a little more than in the main patch. It is seen that the decay rate was similar in all the small patches. Decay rate increased with time when

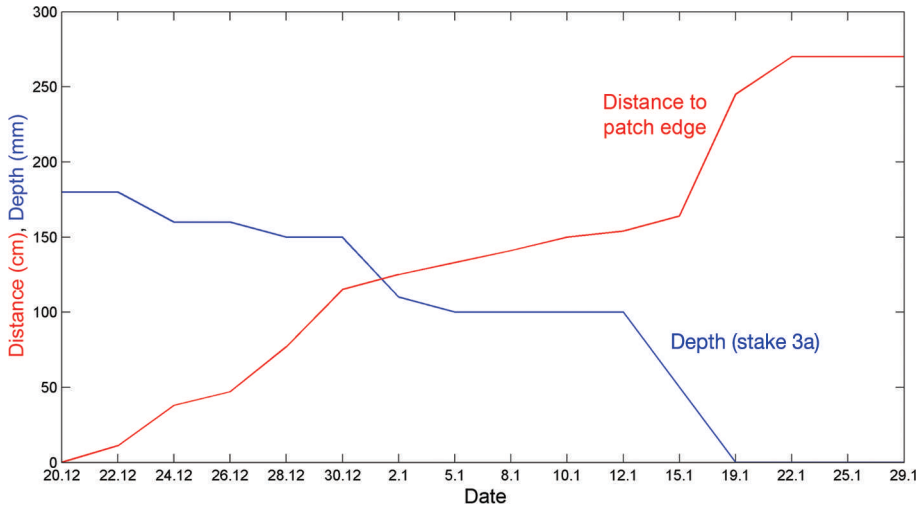

Fig. 7. The evolution of the edge of the snowpatch near stake 3a. The distance of the edge to a fixed marker and snow depth at a fixed stake are shown. The initial time is 20 December 2010. Date format is day.month.

https://doi.org/10.3189/2013JoG12J236 Published online by Cambridge University Press

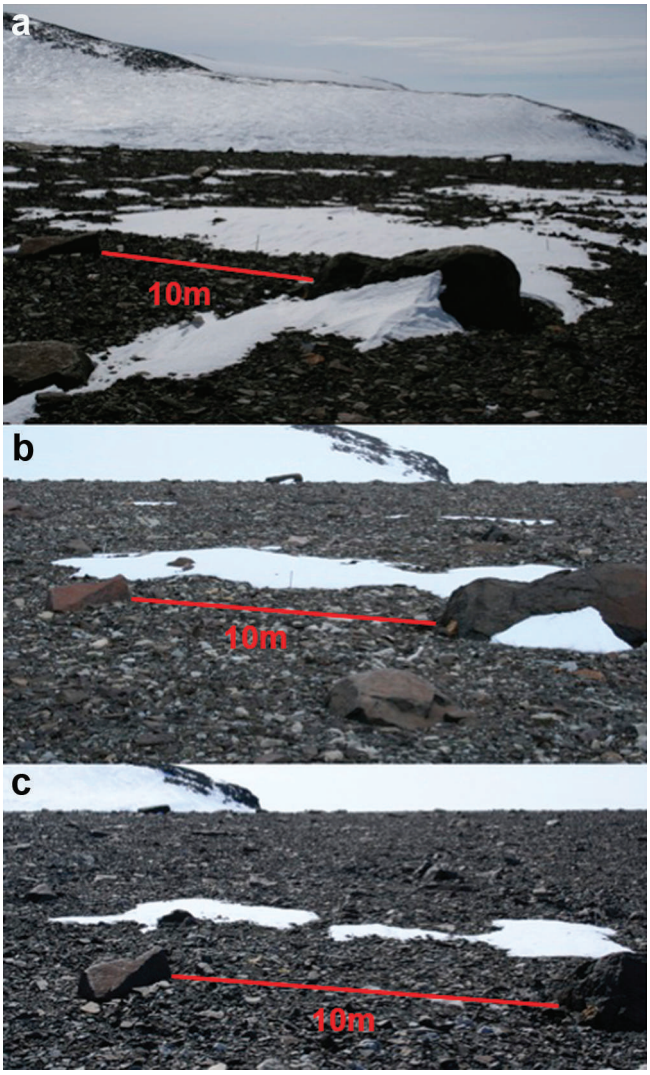

Fig. 8. Photographs of one small snowpatch (initially ~20 m^2) on (a) 6 December, (b) 14 December and (c) 23 December 2010 in the study area.

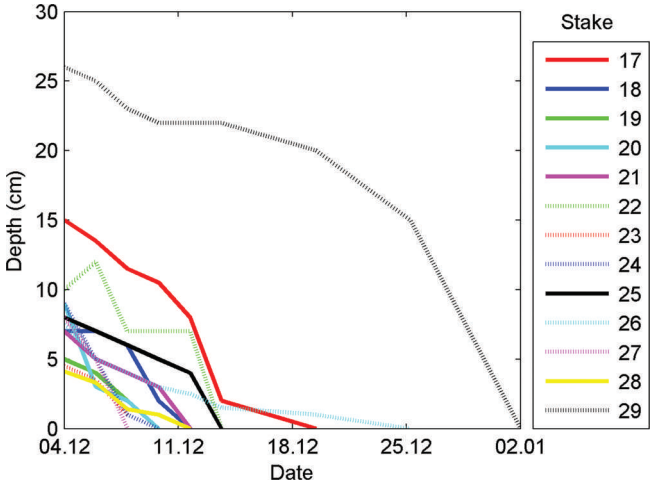

Fig. 9. Decay of the small snowpatches in December 2010–January 2011. The thickness of snow at the stake in the centre of each patch is presented. Date format is day.month.

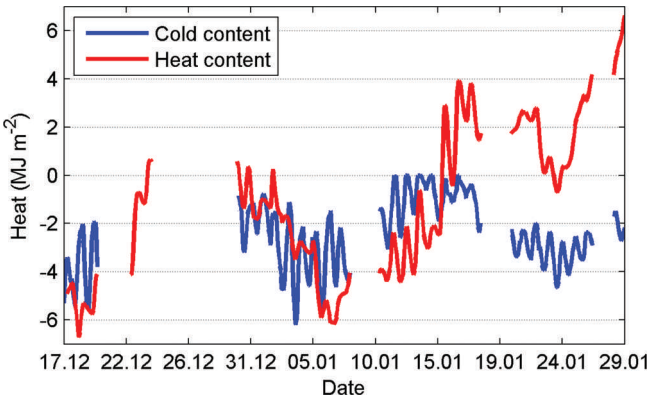

Fig. 10. The heat storage of the snowpack in December 2004–January 2005. Cold content is proportional to the mean snow temperature, and heat content is the initial value plus the time integral of the external heat fluxes. At data gaps the level is kept constant; this shifts cold content correctly, but heat flux integration may lose the level and should be examined only for the changes during periods with continuous data. Date format is day.month.

snow became thin due to the feedback from the warming of the soil underneath. Both melting and sublimation took place during the decay process.

Assuming the vertical decay rate is 7.5 mm d^{-1} and the duration of the summer is 60 days, the total decay of snow is 450 mm. Thus the minimum thickness of snowpatches to survive over summer and become perennial is ~500 mm at the beginning of summer. At the margin of snowpatches the snow thickness slopes down by ~1 : 10 and the edge decays by 10 cm d^{-1}. Consequently, to have sufficient vertical and lateral extent to survive over the summer, a snowpatch needs to have a diameter >10 m. Since perennial patches need annual non-negative net snow accumulation, their lifetime is sensitive to changing wind and snowfall conditions.

4. HEAT BALANCE OF SNOW

4.1. Cold content of snowpack

The heat content of a snow layer (U) can be expressed as

$$U - U_0 = \int_0^h \rho_s c T \, \mathrm{d}z + \rho_s L_f \nu h \qquad (5)$$

where U_0 is the reference level, here equal to the heat content of the snowpack in solid state at 0°C, c is the specific heat of ice, T is the temperature, L_f is the latent heat of freezing and ν is the liquid water content of snow. The representative snow thickness of the main snowpatch was 500 mm. The first term on the right-hand side is the cold content of the snowpack, denoted by F_d. It was estimated by using a constant reference density for snow and integrating the temperature profile with the trapezoidal rule. In summer 2004/05, the cold content was initially –4 MJ m^{-2}, reaching zero on 10–15 January and decreasing to –2 MJ m^{-2} at the end of January (Fig. 10). The cold content indicates the sensible heat storage of the snowpack; it is proportional to the mean temperature of snow. The second term represents the latent heat of the liquid water within the snow cover. This term accounted for <0.5 MJ m^{-2} in the present case, since the liquid water content was <1%.

Initially, the mean snow temperature was –7.5°C and in the summer the snow achieved isothermal melting stage

https://doi.org/10.3189/2013JoG12J236 Published online by Cambridge University Press

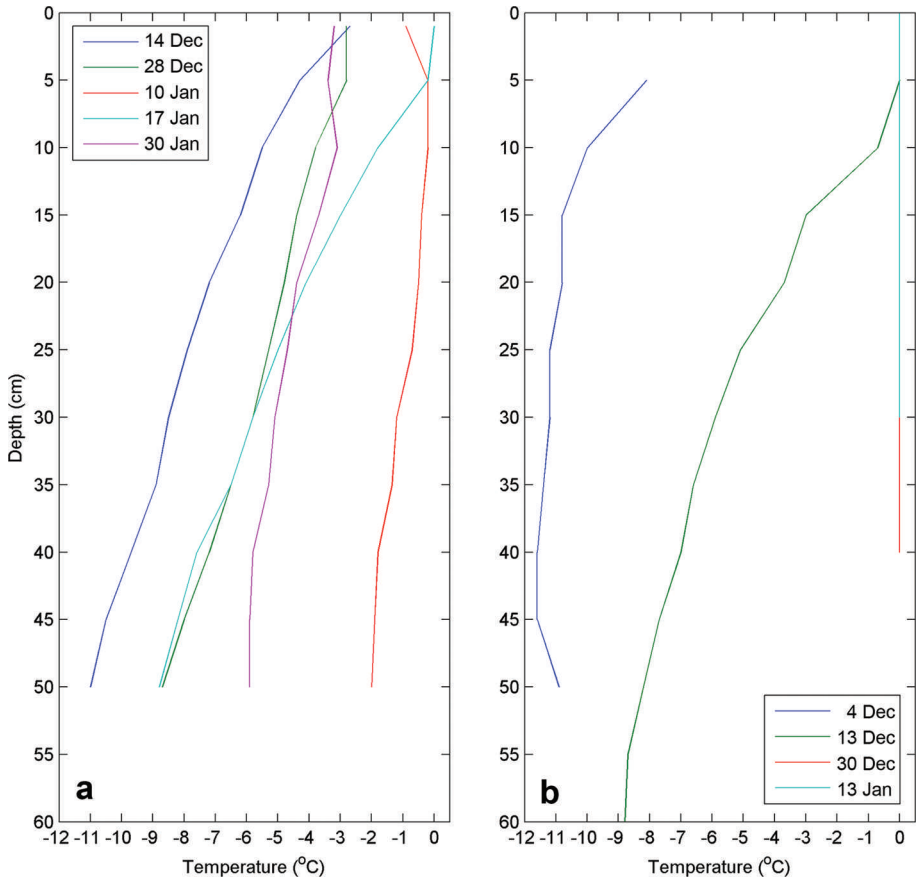

Fig. 11. Vertical profiles of temperature at the snow site in summer (a) 2004/05 and (b) 2010/11. In the latter season, the snowpack was isothermal at 0°C from 30 December.

(Fig. 11). At the peak of the summer (10 January), the temperature increased to nearly 0°C across the snowpack. Cooling started after 20 January. In the earlier season the temperature gradient was ~0.2°C cm^{-1}, corresponding to a heat loss of 5–10 W m^{-2} from the snowpack to the ground. In summer 2010/11 the temperature of the snowpack increased to 0°C throughout at the end of December. The early-season temperature profiles were similar to those in 2004/05.

4.2. Heat balance

Accumulation of heat into the snowpack is obtained from the heat balance equation (e.g. DeWalle and Rango, 2008):

$$\frac{\mathrm{d}U}{\mathrm{d}t} = Q_{\mathrm{Rad}} - \rho_{\mathrm{w}} L_{\mathrm{s}} E + Q_{\mathrm{c}} + Q_{\mathrm{P}} + Q_{\mathrm{g}} \qquad (6)$$

where Q_{Rad} is the radiation balance, L_{s} is the latent heat of sublimation, Q_{c} is the sensible heat flux, Q_{P} is the heat flux due to precipitation and Q_{g} is the heat flux from the ground. The leading terms are the radiation balance and the latent heat flux. Precipitation brings a significant amount of heat when it falls in liquid state into cold snow but this did not take place in the present experiments. The heat flux from the ground was estimated using the temperature gradient at the bottom of the snowpack and the thermal conductivity of snow. It was negative in summer under the main snowpatch, i.e. solar and atmospheric heat was transferred through snow to the ground.

Using Eqn (6), the evolution of the heat content (relative to the solid phase of water at 0°C) was obtained from the meteorological observations by time integration, starting from the actual heat content measured at the beginning. In cold snow, this heat content integral is equal to the cold content of snow, and when the snowpack has reached the melting point, the heat content becomes positive and increases with liquid water formation (Fig. 10). Owing to technical problems in the AWS, there were a few data gaps of 1–2 days, which were considered too long for interpolation. For simplicity the heat flux integral was assumed zero over each gap. This assumption was reasonable except for the latter half of January, which most likely led to a positive bias.

Consequently, only the evolution of the curves for the cold content and heat content during continuous data periods should be compared. This comparison is quite good. After 15 January, the heat content was positive due to liquid water formation and this is not included in the definition of the cold content. At the 19 January data gap the heat content most likely decreased rather than kept the assumed zero and therefore the curves depart thereafter. Still both curves show similar behaviour, decreasing to 24 January and then increasing toward the end of the month. The changes were stronger in the flux integration, since that includes melting and refreezing. The heat required to melt a 1 cm liquid water layer from snow is 3.35 MJ m^{-2} and the heat content suggested approximately this much liquid water was available in mid-January. The direct snow-pit measurements showed that the volume fraction of liquid water was <1%, suggesting that the maximum heat content of the snowpack was <1 MJ m^{-2}.

Radiation had a dominant role in the heat budget. The radiation balance can be written as (e.g. Curry and

https://doi.org/10.3189/2013JoG12J236 Published online by Cambridge University Press

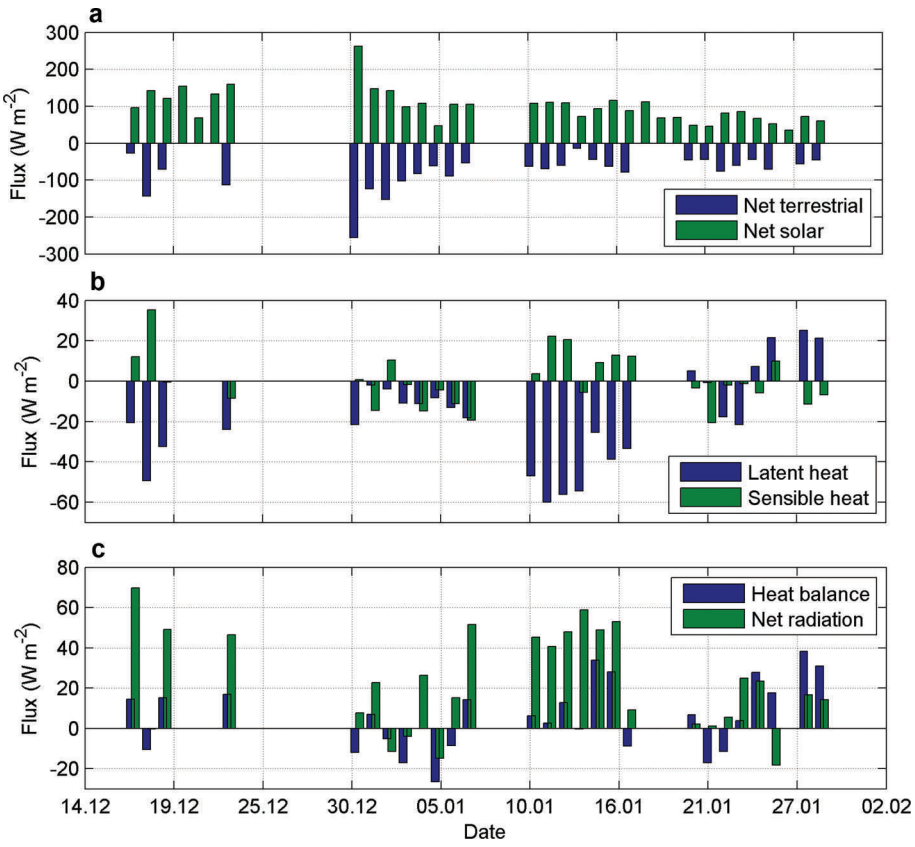

Fig. 12. Daily averages of (a) net solar radiation and net terrestrial radiation, (b) sensible and latent heat fluxes and (c) net radiation and heat balance during December 2004–January 2005. Date format is day.month.

Webster, 1999)

$$Q_{\mathrm{Rad}} = Q_{\mathrm{s}} - Q_{\mathrm{r}} + Q_{\mathrm{L,a}} - Q_{\mathrm{L,s}} \qquad (7)$$

where Q_{s} is the incoming solar radiation, Q_{r} is the outgoing solar radiation, $Q_{\mathrm{L,a}}$ is the incoming terrestrial radiation and $Q_{\mathrm{L,s}}$ is the outgoing terrestrial radiation. The radiation balance and the solar radiation terms were measured and the outgoing terrestrial radiation was obtained from the grey body law with emissivity equal to 0.97. The radiation emitted by the atmosphere can then be estimated from Eqn (7). The measured terms are accurate to 5 W m^{-2}. The outgoing terrestrial radiation has a similar accuracy as the surface temperature is considered to be accurate to within 1°C, so the incoming terrestrial radiation obtained as the residual has a low accuracy, of the order of 20 W m^{-2}.

Figure 12 shows the daily heat balances, and Table 2 shows their statistics. The mean values of the incoming and outgoing solar radiation were 311.4 and –212.3 W m^{-2}, respectively, and the overall albedo was 68%. This albedo is much less than on the neighbouring ice sheet, possibly due to the presence of surface soil particles transported from snow-free spots. Also, toward the end of the measurement period, snow became thinner so that radiation was also absorbed by the soil surface. The highest values of incoming solar radiation (~700 W m^{-2}) were measured at noon in clear-sky conditions, and the lowest noon values were 400 W m^{-2} on cloudy days. The net terrestrial radiation was –80.9 W m^{-2}, equal to the difference between the emission from the snow surface (–287.1 W m^{-2}) and the emission from the atmosphere (206.1 W m^{-2}). The net terrestrial radiation did not fluctuate as much as the net solar radiation. Note that the net radiation and net solar radiation were measured directly, so the net terrestrial radiation is the difference of the measured data. The distribution of the net terrestrial radiation to incoming and outgoing parts contains assumptions and thus larger uncertainties.

The turbulent fluxes of sensible and latent heat were calculated using the method of Launiainen and Vihma (1990), which accounts for the stability of the stratification in the atmospheric surface layer, as described in Section 3.1. The variability of both fluxes was high (Fig. 12; Table 2). The strongest fluxes were measured in mid-January, when the sensible heat flux peaked at 20 W m^{-2} and the latent heat flux at –50 W m^{-2}. The sensible heat flux averaged approximately zero (0.2 W m^{-2}) with a large diurnal variability, but

Table 2. Statistics of the daily surface heat fluxes in summer 2004/05 (W m^{-2}). The solar radiation that penetrated into the snow is included in the net solar radiation row

	Average	Standard deviation	Minimum	Maximum
Incoming solar radiation	311.4	230.4	127.2	481.3
Outgoing solar radiation	–212.3	163.3	–301.1	–74.6
Net solar radiation	99.1	94.5	35.0	262.8
Outgoing terrestrial radiation	–286.0	14.1	–297.1	–272.1
Incoming terrestrial radiation	207.1	82.6	128.1	283.8
Net terrestrial radiation	–78.9	79.9	–153.1	–13.2
Radiation balance	20.2	73.3	–18.3	69.7
Latent heat flux	–15.5	24.9	–60.0	25.2
Sensible heat flux	0.2	28.9	–20.6	35.3
Surface heat balance	4.9	50.2	–26.4	38.3

https://doi.org/10.3189/2013JoG12J236 Published online by Cambridge University Press

the average latent heat flux was –15.5 W m^{-2}. At the end of January the latent heat flux showed positive values, i.e. deposition of water vapour on the surface. In summer 2004/05, the net solar and terrestrial radiation and the latent heat flux were clearly the dominant terms (Table 2).

The mean radiation balance was 20.2 W m^{-2} and the maximum value was measured in mid-January (Fig. 12; Table 2). The mean level corresponded to heat accumulation of 1.7 MJ m^{-2} d^{-1}. The radiational heat gain was largely compensated by the latent heat flux. The mean values of the sensible and latent heat fluxes were 0.2 and –15.5 W m^{-2}, respectively. The heat flux to the ground was very small (not shown in the plot); the range was from –3 to 8 W m^{-2} and the mean value was 1.5 W m^{-2}.

The surface heat balance was positive in the afternoons and negative at nights, the overall average being 4.9 W m^{-2}. This left power of 3.4 W m^{-2} for warming and melting of the snowpack. At the beginning, the mean temperature of the snowpack was –7.5°C and with the given power it would take 11 days to raise the temperature of the snow to 0°C, leaving energy to produce ~3 cm of meltwater. This is biased up, since the integration of the heat content of snow resulted in a 1 cm level of meltwater, and that method is more accurate than the flux method. Still, the agreement is good and it is clear that the net heat gain of the snowpatch could not produce much melt and the mass loss took place primarily by sublimation. The good accuracy of the flux method here is due to the measurement of net radiation directly.

The surface layer of the bare frozen ground melted to 0.5 m depth. The surface temperature of the bare ground was >10°C on sunny days.

4.3. Penetration of solar radiation in the snowpack

Attenuation of downwelling irradiance in the snowpack is modelled here using an attenuation law analogous to the Bouguer–Lambert absorption law (Warren, 1982), where irradiance decreases with depth in proportion to the diffuse extinction coefficient $k = k(z)$. The solution is given by

$$E_{\mathrm{d}}(z) = E_{\mathrm{d}}(h^{-}) \exp\left[-\int_{z}^{h} k(z')\,\mathrm{d}z'\right] \qquad (8)$$

where E_{d} is the downwelling PAR irradiance and h^{-} refers to the level just below the snow surface. Equation (8) can be used to estimate the mean extinction coefficient between two measurement depths. The PAR data were used to estimate the extinction coefficient.

On the snow surface, the directional distribution of the incoming radiance depends primarily on the Sun's position and the cloudiness. In overcast conditions irradiance is practically diffuse at the surface, and, in general, due to strong scattering of light in the snowpack, the irradiance is always diffuse a little below the surface. In a thin top layer the extinction coefficient depends on the depth, but deeper it approaches a diffuse, asymptotic level. According to Warren and others (2006), usually ~1 cm is a sufficient depth to achieve the asymptotic state, depending on the physical properties of the snow. Irradiance normally decreases faster in the top layer than in the asymptotic zone (Bohren and Barkström, 1974), and in the asymptotic zone the extinction coefficient depends only on snow properties.

In summer 2004/05 the PAR sensors were deployed on 17 December and retrieved on 21 December. One sensor was deployed to a depth of 10 cm and another sensor was mounted above the snowpack. They recorded the incoming quantum irradiance at 10 min intervals (Fig. 13). During this 4 day period the snow surface decreased by 5 mm. The decrease in the snow surface was observed from the snowline stakes 5 and 6 a few metres away from the sensors. The mean value of the extinction coefficient was 0.113 cm^{-1}, and the extremes (0.07 and 0.187 cm^{-1}) were obtained at night, but these values are uncertain because of the high sensitivity of the PAR measurements to low solar angles (Fig. 13). The critical elevation, below which the extinction coefficient started to vary widely, was ~12°. The mean extinction coefficient was 0.105 cm^{-1} for higher solar altitudes. Thus the penetration depth of sunlight was 25–30 cm, when defined as three times the inverse extinction coefficient to correspond to the total attenuation of 95%. When snow is thinner, sunlight starts to warm the soil below the snow, bottom melting begins and the decay is accelerated.

The average net solar radiation was 99.1 W m^{-2}. About 50% of the solar heating comes from the visible light band, which can penetrate the snowpack. Here most of this heat was lost to the atmosphere by conduction; however, where the thickness of the snow was <100–150 mm, >10 W m^{-2} reached the snow–soil interface and could be used to a large extent to melt snow at the bottom, by 1–2 mm SWE d^{-1}. For the observed lateral decay of the snowpatch (10 cm d^{-1}), heating by 10–20 W m^{-2} is required. This power magnitude is obtained from the sunlight. Heat is also conducted laterally to the edge of the snowpatch in the bare ground. Taking the lateral temperature gradient as 5°C m^{-1} in the 10 cm surface layer, corresponding to occasional field measurements, and the thermal conductivity of the gravel ground as ~5 W m^{-1} °C^{-1}, then the lateral heat conduction to the edge of snowpatches is ~2.5 W m^{-2}, much less than what is brought in directly by the sunlight.

5. CONCLUSIONS

The mass and heat balance of snowpatches has been investigated at Basen nunatak in the austral summers (December–January) of 2004/05 and 2010/11. Snow thickness decreased by 230 mm between these summers, and in the latter summer more snow mass was lost due to sublimation and runoff. Direct measurements of the mass balance, heat content and fluxes were made to obtain a good picture of the nunatak snow decay in summer.

Snow thickness decreased on average by 5 mm d^{-1} (2 mm SWE d^{-1}), and up to half of the decrease was due to metamorphic compression of the snow cover; the rest was loss of mass by sublimation and runoff. In 2004/05 the rate of decrease of snow thickness was 4 mm d^{-1} and in 2010/11 it was 6.3 mm d^{-1}. Thin snow cover decayed faster, since solar heating of the ground can initiate snowmelt at the bottom of the snow cover. Lateral decay due to sublimation and melting shrunk normal snowpatches by 10 cm d^{-1}, mainly due to the energy from sunlight penetrating through thin snow to the ground. Also, conduction of heat from bare ground to the edge of snowpatches was significant. Runoff of meltwater, formed at the bottom of thin snow, may form drainage systems with ponds and serve as the source of water for soil and pond ecosystems.

The surface heat balance of snowpatches was only slightly positive, sufficient to remove the cold content from the snow cover but, in addition, only a marginal amount of meltwater, of the order of 10 mm SWE. The average heat

https://doi.org/10.3189/2013JoG12J236 Published online by Cambridge University Press

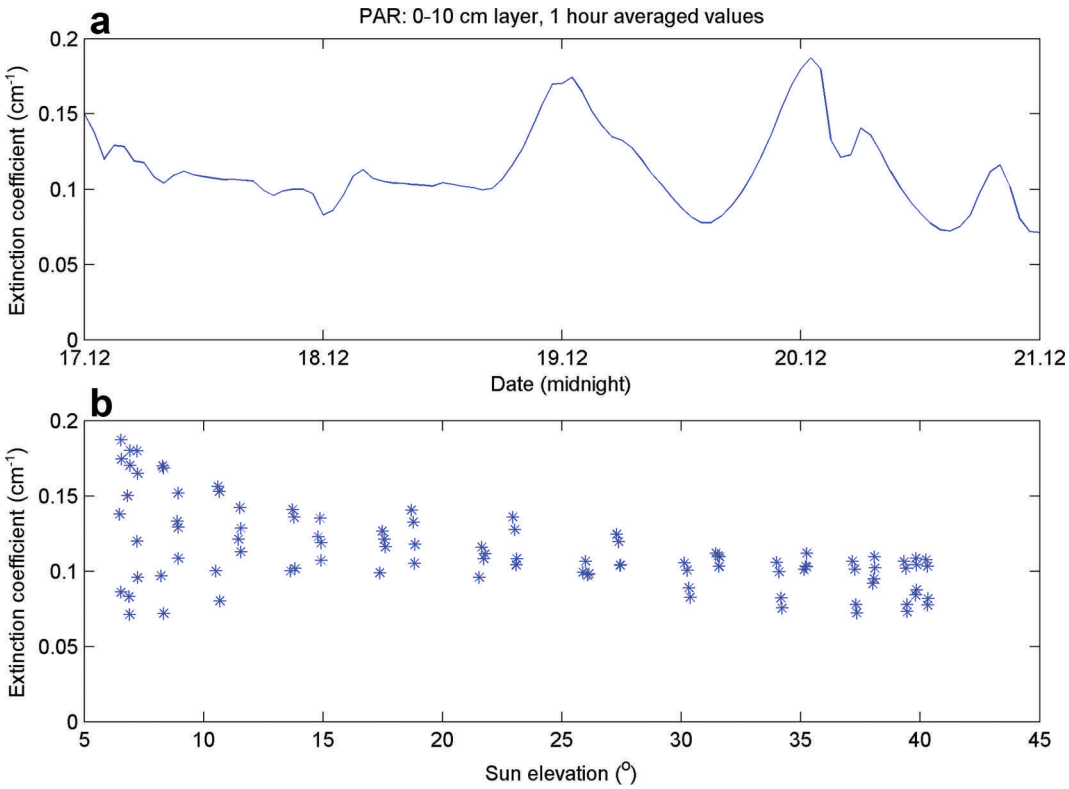

Fig. 13. (a) The time evolution of the extinction coefficient in the snowpack during 17–21 December 2004. Date format is day.month. (b) Extinction coefficient versus solar altitude.

balance was dominated by net solar radiation (99.1 W m^{-2}) and net terrestrial radiation (–78.9 W m^{-2}), resulting in the net radiation balance of 20.2 W m^{-2}. The average latent heat flux was –15.5 W m^{-2}, while the sensible heat flux averaged almost zero (0.2 W m^{-2}). The mean surface heat flux was 4.9 W m^{-2} and the heat flux to the ground from the snowpack was 1.5 W m^{-2}. Net radiation was measured directly and the main uncertainties in the heat balance were concerned with the estimation of the turbulent fluxes.

Direct measurements of the mass balance using snow stakes and snow pits and indirect measurements based on the heat balance were consistent with each other. Also, the heat content measurements, directly from snow temperature profiles and indirectly from the heat fluxes, showed consistency.

Summer 2010/11 was clearly warmer than summer 2004/05. In 2010/11 the temperature of the whole snowpack had risen to the melting point at the end of December. During summer 2004/05 the temperature of the snow was highest on 17 January with minimum at –2°C. In December 2010 the rate of decrease of snow thickness was approximately double that in December 2004. In January 2011 the rate was slightly higher than in January 2005. The physical properties of the snowpack were different between the summer seasons. One reason for this is probably the major rainfall event that occurred in January 2010. FINNARP records show that in January 2003 there was another rainfall event, but these are the only two events that have been recorded since the mid-1990s.

Small snowpatches on the nunatak are dynamic. The rate of lateral decay of minor patches (<10 m^2) was ~10 cm d^{-1}. Snowpatches thicker than 40–50 cm and wider than 10 m may survive over summer. Thin snow decayed faster due to surface thermomechanical erosion and also melted from the bottom when the soil was warmed by the solar radiation. At a snow thickness of 25–30 cm the ground begins to warm, corresponding to penetration depth of solar radiation (defined as three e-folding depths equal to the reduction to 5% from the level just below the surface), and then also the penitents start to reach the ground.

The mass balance of nunatak snowpatches influences the ice sheet around them due to sublimation, runoff and snowdrift. There is also a local positive feedback between the decay of snowpatches and the heat balance of nunataks caused by the albedo. It can be anticipated that the snowpatches on nunataks are sensitive to climate variations, but this question requires more investigation with longer time series.

ACKNOWLEDGEMENTS

Discussions with Hardy B. Granberg are greatly appreciated. We thank Mika Kalakoski and Olli-Pekka Mattila for help with the fieldwork. This research was financed by the Academy of Finland, projects Seasonal snow in Antarctica (54086) and Evolution of snow cover and dynamics of atmospheric deposits in the snow in Antarctica (127691).

REFERENCES

Berrisford MS (1991) Evidence for enhanced mechanical weathering associated with seasonally late-lying and perennial snow patches, Jotunheimen, Norway. *Permafrost Periglac. Process.*, **2**(4), 331–340 (doi: 10.1002/ppp.3430020408)

Bohren CF and Barkström BR (1974) Theory of the optical properties of snow. *J. Geophys. Res.*, **79**(30), 4527–4535 (doi: 10.1029/JC079i030p04527)

https://doi.org/10.3189/2013JoG12J236 Published online by Cambridge University Press

Curry JA and Webster PJ (1999) *Thermodynamics of atmospheres and oceans*. (International Geophysics Series 65) Academic Press, London

DeWalle DR and Rango A (2008) *Principles of snow hydrology*. Cambridge University Press, Cambridge

Eurola S, Huttunen S and Welling P (2004) *Floristic statistics of the fjelds of NW Enontekiö, Finnish Lapland (68°45′–69°17′N; 20°45′–22°E)*. (Kilpisjärvi Notes 18) Kilpisjärven Biological Station, Helsinki [in Finnish with English summary] http://www.helsinki.fi/kilpis/english/research/notes_eng.htm

Fierz C and 8 others (2009) *The international classification for seasonal snow on the ground*. (IHP Technical Documents in Hydrology 83) UNESCO–International Hydrological Programme, Paris

Gooseff MN and 8 others (2003) Snow-patch influence of soil biogeochemical processes and invertebrate distribution in the McMurdo Dry Valleys, Antarctica. *Arct. Antarct. Alp. Res.*, **35**(1), 91–99

Granberg HB, Cliche P, Mattila OP, Kanto E and Leppäranta M (2009) A snow sensor experiment in Dronning Maud Land, Antarctica. *J. Glaciol.*, **55**(194), 1041–1051 (doi: 10.3189/002214309790794823)

Ingvander S, Brown I and Jansson P (2011) Spatial snow grain size variability along the JASE 2007/2008 traverse route in Dronning Maud Land, Antarctica, and its relation to MOA NDSI index, MEDRIS and MODIS satellite data. In Lacoste-Francis H ed. *Proceedings of ESA Living Planet Symposium: 28 June–2 July 2010, Bergen, Norway*. (ESA Proceedings SP-686) European Space Agency, Noordwijk

Isaksson E and Karlén W (1994) Spatial and temporal patterns in snow accumulation, western Dronning Maud Land, Antarctica. *J. Glaciol.*, **40**(135), 399–409

Kanto E, Leppäranta M and Mattila O-P (2007) *Seasonal snow in Antarctica. Data report II*. (Report Series in Geophysics 55) Department of Physics, University of Helsinki, Helsinki

Kärkäs E (2004) Meteorological conditions of the Basen Nunatak in western Dronning Maud Land, Antarctica, during the years 1989–2001. *Geophysica*, **40**(1–2), 39–52

Kärkäs E, Granberg HB, Kanto K, Rasmus K, Lavoie C and Leppäranta M (2002) Physical properties of the seasonal snow cover in Dronning Maud Land, East Antarctica. *Ann. Glaciol.*, **34**, 89–94 (doi: 10.3189/172756402781817554)

Keskitalo J, Leppäranta M and Arvola L (2013) First records of primary producers of epiglacial and supraglacial lakes in western Dronning Maud Land, Antarctica. *Polar Biol.*, **36**(10), 1441–1450 (doi: 10.1007/s00300-013-1362-0)

Launiainen J and Vihma T (1990) Derivation of turbulent surface fluxes – an iterative flux-profile method allowing arbitrary observing heights. *Environ. Softw.*, **5**(3), 113–124 (doi: 10.1016/0266-9838(90)90021-W)

Leppäranta M and Myrberg K (2009) *Physical oceanography of the Baltic Sea*. Springer Praxis, Berlin.

Lliboutry L (1954) The origin of penitents. *J. Glaciol.*, **2**(15), 331–338

Mott R, Gromke C, Grünewald T and Lehning M (2013) Relative importance of advective heat transport and boundary layer decoupling in the melt dynamics of a patchy snow cover. *Adv. Water Resour.*, **55**, 88–97 (doi: 10.1016/j.advwatres.2012.03.001)

Parish TR (1988) Surface winds over the Antarctic continent: a review. *Rev. Geophys.*, **26**(1), 169–180 (doi: 10.1029/RG026i001p00169)

Paterson WSB (1994) *The physics of glaciers*, 3rd edn. Elsevier, Oxford

Pihkala P and Spring E (1985) *A practical method for photographing snow samples*. (Report Series in Geophysics 20) Department of Geophysics, University of Helsinki, Helsinki

Reijmer CH and Van den Broeke MR (2003) Temporal and spatial variability of the surface mass balance in Dronning Maud Land, Antarctica, as derived from automatic weather stations. *J. Glaciol.*, **49**(167), 512–520 (doi: 10.3189/172756503781830494)

Richardson-Näslund C (2004) Spatial characteristics of snow accumulation in Dronning Maud Land, Antarctica. *Global Planet. Change*, **42**(1–4), 31–43

Sihvola A and Tiuri M (1986) Snow fork for field determination of the density and wetness profiles of a snow pack. *IEEE Trans. Geosci. Remote Sens.*, **24**(5), 717–721 (doi: 10.1109/TGRS.1986.289619)

Van den Broeke MR and Bintanja R (1995) The interaction of katabatic winds and the formation of blue-ice areas in East Antarctica. *J. Glaciol.*, **41**(138), 395–407

Warren SG (1982) Optical properties of snow. *Rev. Geophys.*, **20**(1), 67–89 (doi: 10.1029/RG020i001p00067)

Warren SG, Brandt RE and Grenfell TC (2006) Visible and near-ultraviolet absorption spectrum of ice from transmission of solar radiation into snow. *Appl. Opt.*, **45**(21), 5320–5334 (doi: 10.1364/AO.45.005320)

Watson A, Davison RW and French DD (1994) Summer snow patches and climate in northeast Scotland, UK. *Arct. Alp. Res.*, **26**(2), 141–151

MS received 15 December 2012 and accepted in revised form 20 August 2013